CHEMISTRY OF MATERIALS

ARTICLE

pubs.acs.org/cm

Nonsymmetric bent-core liquid crystals based on a 1,3,4-thiadiazole core unit and their nematic mesomorphism

Jens Seltmann,[†] Alberto Marini,[‡,§] Benedetta Mennucci,[‡] Sonal Dey,[⊥] Satyendra Kumar,[⊥] and Matthias Lehmann*[,†,#]

[†]Institute of Chemistry, Chemnitz University of Technology, Strasse der Nationen 62, 09111 Chemnitz, Germany

[#]Institute of Organic Chemistry, University of Würzburg, Am Hubland, 97074 Würzburg, Germany

[‡]Dipartimento di Chimica e Chimica Industriale, Università di Pisa, via Risorgimento 35, 56126 Pisa, Italy

[⊥]Department of Physics, Kent State University, Kent, Ohio 44242, United States

ABSTRACT: The synthesis and thermotropic properties of novel V-shaped molecules having a central 1,3,4-thiadiazole core with a bend-angle of 160° are reported. The compounds consist of a shape-persistent oligo(phenylene ethynylene) scaffold with lateral alkyloxy substituents. One of the terminal aromatic units possesses an alkoxy chain capped by an ethyl ester group while the second terminus is a pyridyl group. They exhibit enantiotropic nematic phases and are characterized by polarized optical microscopy, differential scanning calorimetry, and X-ray diffraction. Results from conoscopy indicate a biaxial nature of the nematic phase near room temperature. DFT calculations of dipole moments and molecular polarizabilities are used to substantiate the experimental findings.

KEYWORDS: V-shaped nematogens, biaxial nematics, X-ray, conoscopy, DFT calculations

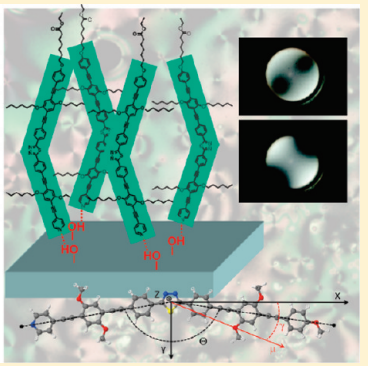

INTRODUCTION

Although the first bent-core liquid crystals (LC) were synthesized in the 1920s by Vorländer,[1] they attracted much attention only in the last fifteen years. Since the report of the existence of new mesophases in banana molecules by Niori et al., ferroelectric, antiferroelectric and ferrielectric behavior of these materials has been established.[2] Theoretical considerations also predicted the existence of the elusive thermotropic biaxial nematic (N_b) phase in bent-core molecules with a specific range of the bend-angle.[3,4] Materials forming such phases are highly attractive not only to elucidate theory, but also for application in a new generation of display technology. The N_b phase was predicted by Freiser[5] in 1970 and subsequently realized in a lyotropic system by Yu and Saupe[6] and in liquid crystalline polymers.[7] Until recently, all endeavors to design thermotropic low molar mass systems led to materials for which the biaxiality could not be substantiated.[8] In 2004, V-shaped oxadiazole derivatives were shown to exhibit the N_b phase at high temperatures by X-ray and ^{2}H NMR spectroscopy.[9,10] Since then, various bent-shape or banana mesogens with flexible molecular scaffolds have been reported to form the N_b phase. However, the exact nature of this phase and the interpretation of results from various methods continue to evolve.[11−14]

We report here the synthesis of unique shape-persistent bent-core liquid crystals. Recently, enantiotropic nematic phases were realized at low temperature in mesogens with a 1,3,4-thiadiazole central core and ethyl (oxyalkyl)carboxylate groups on both terminal aromatic units.[15] The bend-angle θ of approximately 160° deviates from the theoretically predicted angle of 109° for the formation of the N_b phase. However, the large local dipole moment of 1,3,4-thiadiazoles along its bisector (see Table 2) is believed to favor the formation of the N_b phases.[16] We attached a pyridyl group to one of the arms of the molecules **1a**−**d** (Figure 1) instead of an ester terminus. It is known to destabilize the nematic phase and lower the melting point relative to cyano substituted derivatives of this mesogen family.[17] Nevertheless, we were confident to find a stabilization of the mesophases at low temperature owing to the desymmetrisation of the molecules and consequently a weaker crystallization tendency. Additionally, the pyridyl group provides the possibility to supramolecularly modify the molecular structure by hydrogen bonding with an H-bond donor.

EXPERIMENTAL SECTION

Reagents were obtained from Acros and Sigma-Aldrich and used as received. The synthesis of compounds **2**−**4** was described previously.[15,17] The target compounds were obtained by analogous procedures, detailed in reference 15. Column chromatography was carried out on silica 60 (Merck, mesh 70−230). PFT ^{1}H and ^{13}C NMR spectra were recorded in $CDCl_3$ with a Varian Oxford 400 MHz spectrometer with the residual solvent signal at 7.26 ppm as a reference. Mass spectra were obtained on a Finnigan MAT95 (FD MS). Elemental analysis was carried out in the microanalytical laboratory at the University of Mainz. POM observations were made with a Zeiss

Received: January 27, 2011
Revised: April 11, 2011
Published: April 28, 2011

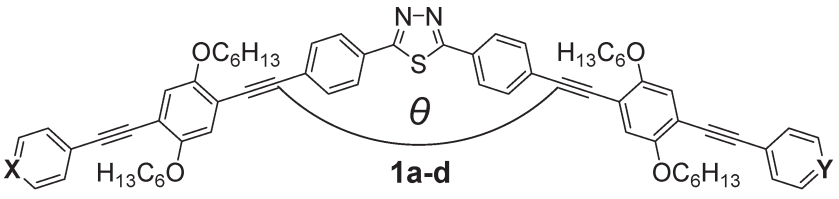

	1e	1f	1g
X	C-O$(CH_2)_4$COOEt	C-O$(CH_2)_6$COOEt	N
Y	C-O$(CH_2)_6$COOEt	C-O$(CH_2)_6$COOEt	N

Figure 1. Target structure of nonsymmetric V-shaped molecules **1a**−**d** and comparable mesogens **1e**−**g** reported previously.[15,17]

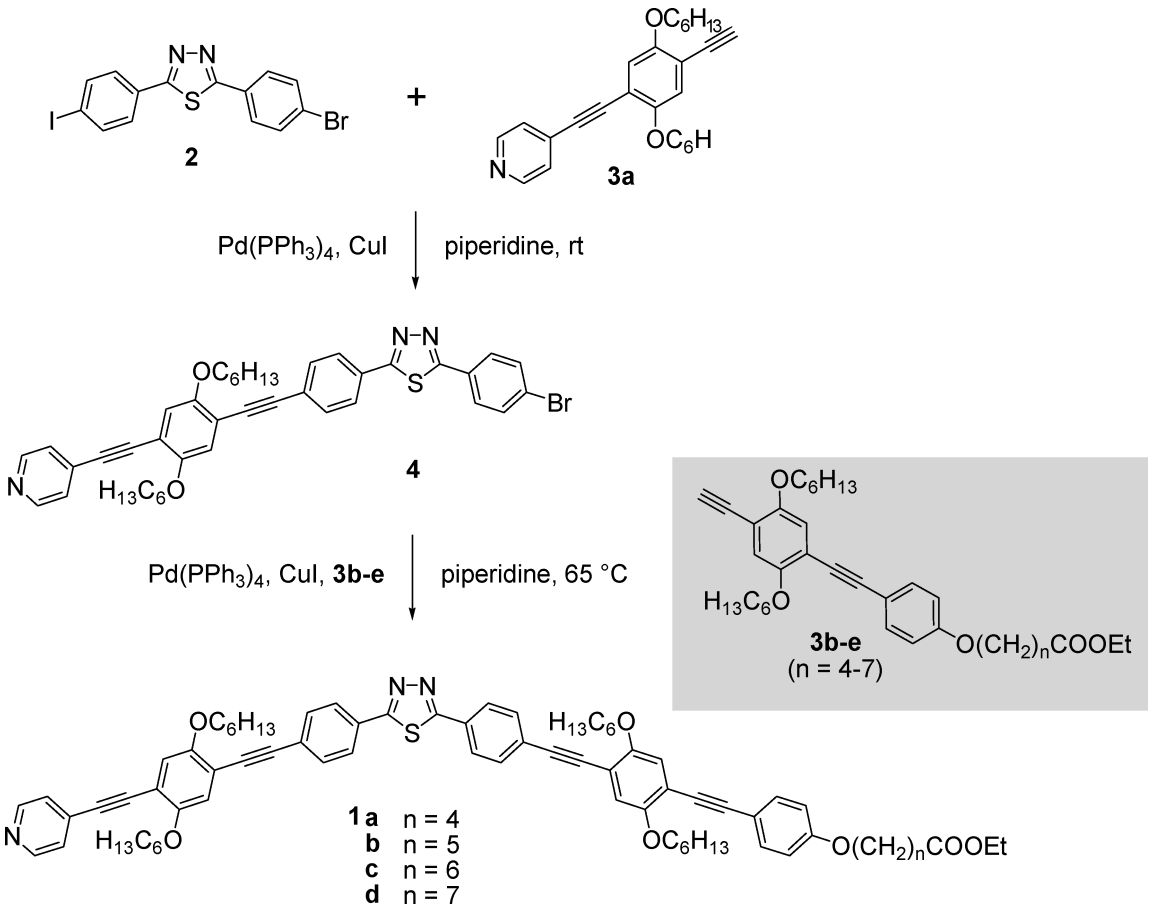

Figure 2. Synthesis of V-shaped thiadiazole derivatives **1a**−**d**.

Axioscop 40 equipped with a Linkam THMS600 hot stage. DSC was performed using a Perkin-Elmer Pyris 1.

Quantum mechanical calculations were performed at in vacuo DFT level of theory, by employing the combination of B3LYP functional and 6-311 g(d,p) basis set. All the calculations were done with the Gaussian 09 package.[18]

X-ray measurements were made at the undulator beamline station 6IDB of the Midwestern Universities Collaborative Access Team's sector at the Advanced Photon Source. A triple bounce Si monochromator was used to select 16.2 keV (λ = 0.76534 Å) X-rays. A pair of X-Y slits was used to collimate the incident X-ray beam to 100 μm × 100 μm. An image plate detector MAR345 was placed at a distance of 506.4 mm from the sample. The incident flux was sufficiently attenuated to avoid radiation damage and to keep the detector from saturating. A silicon standard (NIST 640C) was used to calibrate the spectrometer. Background scattering was recorded using an empty capillary and subtracted from diffraction data. The 2D diffraction patterns thus obtained were used to deduce $2\theta-\theta$ and χ-scans using the Fit2d software package[19] and to calculate the structural parameters and correlations lengths, respectively.

1a. ^{1}**H NMR** (400 MHz, $CDCl_3$): δ [ppm] = 0.91 (m, 12H, CH_3); 1.26 (t, 3H, CH_3, ^3J = 7.2); 1.36 (m, 16H, CH_2); 1.56 (m, 8H, CH_2); 1.84 (m, 12H, CH_2); 2.39 (t, 2H, CH_2COOEt, ^3J = 7.0); 3.96 − 4.08 (m, 10H, OCH_2); 4.12 (q, 2H, $COOCH_2CH_3$, ^3J = 7.2); 6.85 (2H, AA′BB′);

dx.doi.org/10.1021/cm200643u |*Chem. Mater.* 2011, 23, 2630–2636

7.01 (s, 1H); 7.02 (s, 1H); 7.03 (s, 1H); 7.05 (s, 1H); 7.37 (2H, AA′BB′); 7.47 (2H, AA′BB′); 7.63 (4H, AA′BB′); 8.00 (4H, AA′BB′); 8.60 (2H, AA′BB′); **^{13}C NMR** (100 MHz, $CDCl_3$): δ [ppm] = 14.18, 14.21, 14.38 ($\underline{C}H_3$); 21.7, 22.78, 22.80, 25.86, 25.89, 28.7, 29.37, 29.40, 29.43, 29.45, 31.70, 31.75, 34.0 ($\underline{C}H_2$); 60.5 ($COO\underline{C}H_2CH_3$); 67.6; 69.6, 69.7, 69.8 ($O\underline{C}H_2$); 84.7, 88.7, 89.2, 90.7, 92.3, 94.0, 94.7, 95.6 ($\underline{C}\equiv\underline{C}$); 112.9, 113.1 ($C_q$); 114.6 ($C_t$), 114.7 ($C_q$); 115.2, 115.5 ($C_q$); 116.7, 116.8, 117.0 ($C_t$); 125.5 ($C_t$); 126.4, 126.7 ($C_q$); 127.1, 127.94 ($C_t$); 129.5, 129.8, 131.7 ($C_q$); 132.3, 132.4 ($C_t$); 133.2 ($C_t$); 149.9 ($C_t$); 153.5, 153.8, 154.0, 154.1 (C_q, $\underline{C}$-OC_6H_{13}); 159.2 (C_q, $\underline{C}$-OCH_2); 167.7, 167.8 (C_q, N=$\underline{C}$-S); 173.5 (C_q, $\underline{C}$=O); **Elemental anal.** [%] Calcd for $C_{76}H_{85}N_3O_7S$: C 77.06; H 7.23; N 3.55; S 2.71. Found: C 76.86; H 7.27; N 3.53; S 2.73. **FD MS:** m/z [%]: 1183.8 (100, M^+); 1184.8 (66.6, $[M+1]^+$); 1186.0 (24.5, $[M+2]^+$); 1187.7 (16.6, $[M+3]^+$).

Table 1. DSC Data of 1a-g at a Scanning Rate of 10 °C/min

compd	phase transitions[a] (onset (°C)/ΔH (kJ mol^{-1}))	ΔS_N [J mol^{-1} K^{-1}]
1a	**Cr** 109.3/*47.0* **N** 150.3/*0.9* **I**	2.1
1b	**Cr** 98.4/*21.4* **N** 150.2/*0.7* **I**	1.7
1c	**Cr** 90.9/*45.4* **N** 154.7/*0.9* **I**	2.1
1d	**Cr** 105.5/*58.6* **N** 144.6/*0.9* **I**	2.2
1e	**Cr** 68.4/*38.5* **N** 177.7/*1.9* **I**	4.2
1f	**Cr** 98.5/*65.5* **N** 173.9/*1.8* **I**	4.0
1g	**Cr** 141.8/*45.1* (**N** 123.3/*-0.1*)[b] **I**	0.3

[a] Cr crystal, N nematic phase, I isotropic phase; Cr−N transition data is given for the first heating cycle; N−I transition data is reported for the second heating cycle. [b] Data given for the first cooling.[17]

Table 2. DFT Calculated Bend Angle Θ, Dipole Moment Components (μ_X, μ_Y, μ_Z), Modulus (μ), and Angle γ, Formed with Respect to the Longitudinal Axis *X* (see Figure 3 for definition)[a]

	Θ	μ_X	μ_Y	μ_Z	μ	γ
DTPy mod 1	162.1	5.64	3.84	−0.01	6.8	34.2
DTPy mod 2	159.9	5.54	3.87	−0.01	6.8	34.9
1c	159.3	7.41	2.96	0.00	8.0	21.8
1d	159.2	7.00	−0.11	0.15	7.0	1.5
1e	158.3	0.2	4.81	0.02	4.8	87.6

[a] The values relative to angles and dipole moment are expressed in degree (°) and debye (D), respectively.

1b. **^{1}H NMR** (400 MHz, $CDCl_3$): δ [ppm] = 0.90 (m, 12H, $\underline{C}H_3$); 1.26 (t, 3H, $\underline{C}H_3$, ^3J = 7.2); 1.37 (m, 16H, $\underline{C}H_2$); 1.55 (m, 10H, $\underline{C}H_2$); 1.71 (m, 2H, $\underline{C}H_2$); 1.85 (m, 10H, $\underline{C}H_2$); 2.34 (t, 2H, $\underline{C}H_2COOEt$, ^3J = 7.2); 3.98 (t, 2H, $O\underline{C}H_2$, ^3J = 6.4); 4.05 (m, 8H, $O\underline{C}H_2$); 4.13 (q, 2H, $COO\underline{C}H_2CH_3$, ^3J = 7.2); 6.85 (2H, AA′BB′); 7.01 (s, 1H); 7.02 (s, 1H); 7.03 (s, 1H); 7.05 (s, 1H); 7.38 (2H, AA′BB′); 7.45 (2H, AA′BB′); 7.64 (4H, AA′BB′); 8.02 (4H, AA′BB′); 8.61 (2H, AA′BB′); **^{13}C NMR** (100 MHz, $CDCl_3$): δ [ppm] = 14.19, 14.22, 14.4 ($\underline{C}H_3$); 22.8, 24.8, 25.8, 25.9, 29.0, 29.38, 29.42, 29.45, 31.7, 31.8 ($\underline{C}H_2$); 34.4 ($\underline{C}H_2COOEt$); 60.4 ($COO\underline{C}H_2CH_3$); 67.8, 69.70, 69.77, 69.81 ($O\underline{C}H_2$); 84.7, 88.7, 89.2, 90.7, 92.3, 94.0, 94.7, 95.6 ($\underline{C}\equiv\underline{C}$); 112.9, 113.2 ($C_q$); 114.6 ($C_t$); 114.7, 115.2, 115.4 ($C_q$); 116.8, 116.9, 117.0 ($C_t$); 125.6 ($C_t$); 126.4, 126.7 ($C_q$); 128.0 ($C_t$); 129.5, 129.8, 131.7 ($C_q$); 132.36, 132.42, 133.2 (C_t); 149.9 (C_t); 153.6, 153.9, 154.0, 154.1 (C_q, $\underline{C}$-OC_6H_{13}); 159.3 (C_q, $\underline{C}$-OCH_2); 167.7, 167.9 (C_q, N=$\underline{C}$-S); 173.8 (C_q, $\underline{C}$=O); **Elemental anal.** [%] Calcd for $C_{77}H_{87}N_3O_7S$ C 77.16; H 7.32; N 3.51; S 2.68. Found C 76.60; H 7.12; N 3.52; S 2.36. **FD MS**: m/z [%]: 1196.8 (100, M^+); 1197.8 (96, $[M+1]^+$).

1c. **^{1}H NMR** (400 MHz, $CDCl_3$): δ [ppm] = 0.90 (m, 12H, $\underline{C}H_3$); 1.26 (t, 3H, $\underline{C}H_3$, ^3J = 7.2); 1.37 (m, 18H, $\underline{C}H_2$); 1.55 (m, 10H, $\underline{C}H_2$); 1.67 (m, 2H, $\underline{C}H_2$); 1.85 (m, 10H, $\underline{C}H_2$); 2.32 (t, 2H, $\underline{C}H_2COOEt$, ^3J = 7.2); 3.97 (t, 2H, $O\underline{C}H_2$, ^3J = 6.4); 4.05 (m, 8H, $O\underline{C}H_2$); 4.13 (q, 2H, $COO\underline{C}H_2CH_3$, ^3J = 7.2); 6.86 (2H, AA′BB′); 7.01 (s, 1H); 7.02 (s, 1H); 7.03 (s, 1H); 7.05 (s, 1H); 7.38 (2H, AA′BB′); 7.46 (2H, AA′BB′); 7.65 (4H, AA′BB′); 8.02 (4H, AA′BB′); 8.61 (2H, AA′BB′); **^{13}C NMR** (100 MHz, $CDCl_3$): δ [ppm] = 14.2, 14.4 ($\underline{C}H_3$); 22.8, 25.0, 25.88, 25.90, 29.0, 29.2, 29.38, 29.42, 29.5, 31.7, 31.8 ($\underline{C}H_2$); 34.4 ($\underline{C}H_2COOEt$); 60.4 ($COO\underline{C}H_2CH_3$); 68.0, 69.7, 69.76, 69.79 ($O\underline{C}H_2$); 84.7, 88.7, 89.2, 90.8, 92.3, 94.0, 94.8, 95.6 ($\underline{C}\equiv\underline{C}$); 112.9, 113.1 ($C_q$); 114.6 ($C_t$); 114.7, 115.2, 115.4 ($C_q$); 116.8, 116.9, 117.0 ($C_t$); 125.6 ($C_t$); 126.4, 126.7

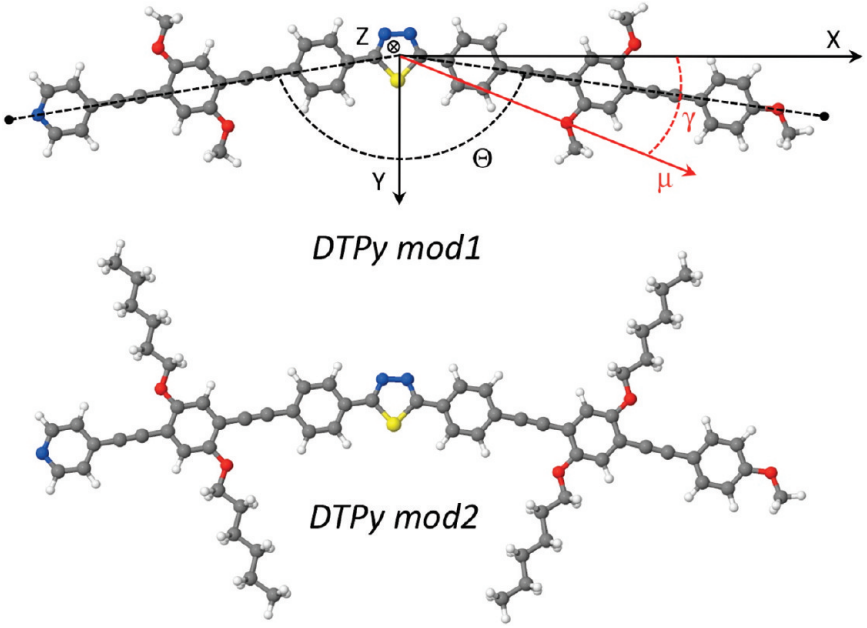

Figure 3. Molecular structures of DTPy models optimized at DFT level. Model 1 and model 2 differ in the length of the lateral aliphatic chains.

(C_q); 128.0 (C_t); 129.5, 129.8, 131.8 (C_q); 132.36, 132.42, 133.2 (C_t); 149.8 (C_t); 153.5, 153.8, 154.0, 154.1 (C_q, C-OC_6H_{13}); 159.4 (C_q, C-OCH_2); 167.7, 167.8 (C_q, N=C-S); 173.9 (C_q, C=O); **Elemental anal.** [%] Calcd for $C_{78}H_{89}N_3O_7S$: C 77.26; H 7.40; N 3.47; S 2.64. Found: C 76.77; H 7.18; N 3.60; S 2.64. **FD MS**: *m*/*z* [%]: 1210.6 (100, M^+); 1211.6 (96, $[M+1]^+$).

1d. ^{1}**H NMR** (400 MHz, $CDCl_3$): δ [ppm] = 0.90 (m, 12H, CH_3); 1.26 (t, 3H, CH_3, ^3J = 7.2); 1.30 − 1.68 (m, 32H, CH_2); 1.75 − 1.90 (m, 10H, CH_2); 2.30 (t, 2H, CH_2-COOEt, ^3J = 7.2); 3.97 (t, 2H, OCH_2, ^3J = 6.4); 4.05 (m, 8H, OCH_2); 4.13 (q, 2H, $COOCH_2CH_3$, ^3J = 7.2); 6.86 (2H, AA′BB′); 7.01 (s, 1H); 7.02 (s, 1H); 7.04 (s, 1H); 7.05 (s, 1H); 7.38 (2H, AA′BB′); 7.46 (2H, AA′BB′); 7.65 (4H, AA′BB′); 8.01 (4H, AA′BB′); 8.61 (2H, AA′BB′); ^{13}**C NMR** (100 MHz, $CDCl_3$): δ [ppm] = 14.2, 14.4 (CH_3); 22.8, 25.0, 25.88, 25.90, 29.0, 29.2, 29.38, 29.42, 29.5, 31.7, 31.8 (CH_2); 34.4 (CH_2COOEt); 60.4 ($COOCH_2CH_3$); 68.0, 69.7, 69.76, 69.79 (OCH_2); 84.7, 88.7, 89.2, 90.8, 92.3, 94.0, 94.8, 95.6 (C≡C); 112.9, 113.1 (C_q); 114.6 (C_t); 114.7, 115.2, 115.4 (C_q); 116.8, 116.9, 117.0 (C_t); 125.6 (C_t); 126.4, 126.7 (C_q); 128.0 (C_t); 129.5, 129.8, 131.8 (C_q); 132.36, 132.42, 133.2 (C_t); 149.8 (C_t); 153.5, 153.8, 154.0, 154.1 (C_q, C-OC_6H_{13}); 159.4 (C_q, C-OCH_2); 167.7, 167.8 (C_q, N=C-S); 173.9 (C_q, C=O); **Elemental anal.** [%] Calcd for $C_{79}H_{91}N_3O_7S$ C 77.35 ; H 7.48 ; N 3.43 ; S 2.61. Found: C 76.79 ; H 7.11 ; N 3.64 ; S 2.75. **FD MS**: *m*/*z* [%]: 1224.6 (100, M^+); 1225.6 (86, $[M+1]^+$).

RESULTS AND DISCUSSION

The synthesis of **1a**-**d** is based on two consecutive Sonogashira Hagihara reactions of different terminal alkyne arms **3a**−**e** with a bromo and iodo substituted 1,3,4-thiadiazole core **2** (Figure 2). The hockey stick compound **4** was first prepared with the pyridyl terminated arm **3a** in a temperature controlled regioselective cross coupling at room temperature (rt).[14,17] Subsequently, the arms **3b**−**e** with a terminal ester group were attached at an elevated temperature of 60 °C to afford the neat target compounds **1a**−**d** in good over all yields of 43−73% (two steps) and high purity.

All molecules show enantiotropic nematic phases with a relatively wide temperature range (Table 1), that can be supercooled to rt. The melting points are lowered from **1a** to **c** and the mesophases' range continuously widens. The nonsymmetric pyridyl derivative **1c** has the lowest melting point and crystallization tendency in the series and the mesophase is indeed more stable at low temperatures when compared to the symmetric compound **1f**. The clearing point indicates an odd−even effect with the number of carbons in the terminal spacers. The enthalpy and entropy changes at the clearing point are comparable to a typical nematic to isotropic (I) transition suggesting a first order transition. In contrast, mesogen **1g**, with two pyridyl groups, exhibits a monotropic phase.[17] Two terminal chains result in enantiotropic mesogens with low melting temperatures dependent on the length of the second alkyl chain (**1e,f**).[17] Evidently, the length of terminal alkyl spacers has important influence on the mesophase stability for this subfamily of shape-persistent bent-core mesogens.

DFT calculations[18] of molecular properties of the symmetric and nonsymmetric mesogens were performed to gain more insight into the influence of the geometry, dipoles, polarizability and molecular biaxiality on the nature and stability of the nematic phases. Tables 2 and 3 summarize the data from simplified molecular models **DTPy mod1,2** (Figure 3) and selected molecules (**1c,d,e**).

The analysis shows that the bend-angle is approximately 159° for almost all mesogens and is slightly influenced by the lateral aliphatic chains (cp. **DTPy mod1**, **DTPymod2** and **1c**). For the symmetric mesogen **1e**, the dipole points almost in the direction of the apex bisector. Molecules **1c** and **1d** possess a considerably larger dipole along the molecule's long axis. However, the angle γ, between the dipole and the molecular *X*-axis, is modified by the length of the terminal spacer. This explains the slight odd−even effect observed for the clearing points of **1a**−**d** (Table 1). As expected the polarizability α is largest along the longitudinal *X*-axis (Table 3). Owing to the large bending angle, the asymmetry parameter $\eta = [(\alpha_{YY} - \alpha_{ZZ})/(\alpha_{XX} - \alpha^{iso})] =$ 0.30−0.44 (α_{XX}, α_{YY}, α_{ZZ} being the principle components of the polarizability tensor and $\alpha^{iso} = (\alpha_{XX} + \alpha_{YY} + \alpha_{ZZ})/3$) is rather small. However, it increases when the lateral chains are attached (cp. **DTPy mod1,2**; Table 3). The asymmetry parameter becomes slightly larger for nonsymmetric compounds **1c,d** (0.41) compared with the symmetric **1e** (0.38).

The nature of the mesophases was first probed with polarized optical microscopy (POM). Compounds **1a**−**d** reveal highly fluid Schlieren textures in the enantiotropic (Figure 4A, B) and monotropic phase regions with integer and half-integer disclinations indicating a nematic phase. On glass substrates, all

Table 3. DFT Calculated Principal Components (α_{XX}, α_{YY}, α_{ZZ}), isotropic component $\alpha^{iso} = (\alpha_{XX} + \alpha_{YY} + \alpha_{ZZ})/3$, anisotropy $\Delta\alpha = [\alpha_{XX} - (\alpha_{YY} + \alpha_{ZZ})/2]$, and Asymmetry, $\eta = [(\alpha_{YY} - \alpha_{ZZ})/(\alpha_{XX} - \alpha^{iso})]$, Parameters Relative to the Molecular Polarizability Tensor, α, in the Cartesian Reference Frame Reported in Figure 3[a]

	α_{XX}	α_{YY}	α_{ZZ}	α^{iso}	$\Delta\alpha$	η_α
DTPy mod 1	2303	618	250	1057	1869	0.30
DTPy mod 2	2511	964	434	1303	1812	0.44
1c	2716	1039	506	1420	1944	0.41
1d	2734	1050	515	1433	1951	0.41
1e	2993	1117	572	1561	2148	0.38

[a] All polarizability components and the anisotropy parameter are expressed in Bohr^3 (with 1 Bohr = 0.52917 Å).

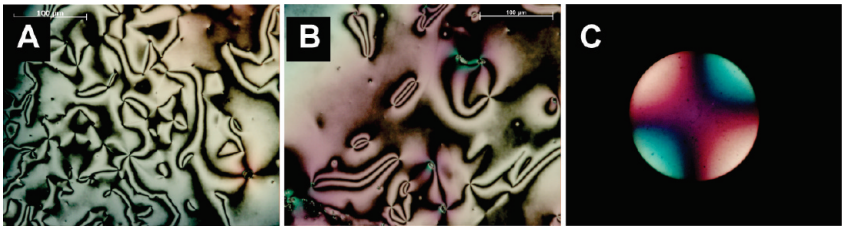

Figure 4. (A, B) Schlieren textures of nematic mesophases of **1c** at 145 °C (A) and **1d** at 67 °C (B). (C) Conoscopic image of the homeotropic aligned sample **1c** at 130 °C with a full wave retardation plate in the light path indicating the optical positive nature of the nematic phase.

dx.doi.org/10.1021/cm200643u |*Chem. Mater.* 2011, 23, 2630–2636

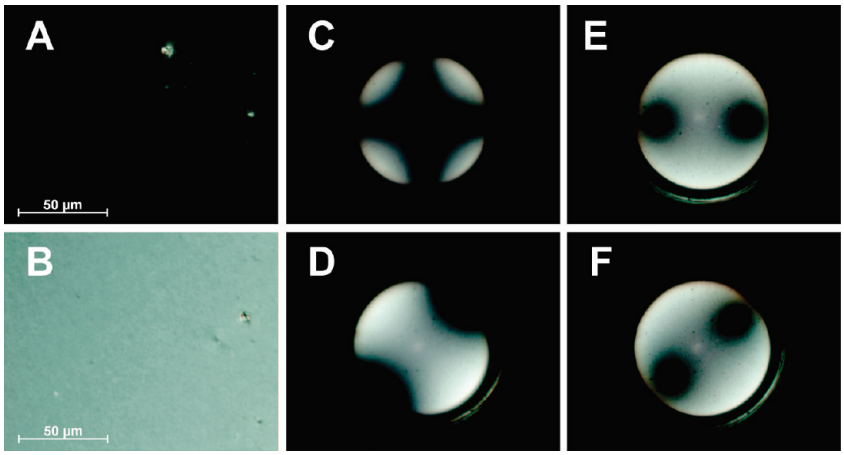

Figure 5. Orthoscopy and conoscopy of homeotropically oriented sample **1c** at rt. Upper row: Sample oriented parallel to the polarizer; lower row: Sample rotated by 45°. (A,B) Orthoscopic images; (C,D) conoscopic observations; (E,F) view on the optical axes by conoscopy using a circular polarizer.

compounds formed large homeotropic areas. Conoscopy, with a full wave retardation plate in the path of light, revealed an optically positive medium (Figure 4C). Because the refractive index is directly proportional to the polarization of the sample, we assume that the molecular long axis (X axis, cp. Figure 3) with the largest polarizability is oriented normal to the substrate. All samples were easily homeotropically aligned on glass presumably due to H-bonding between surface OH-groups and pyridyl H-bond acceptors. The latter was further confirmed by the absence of homeotropic alignment for 1:1 mixtures of pyridyl derivatives with decanoic acid.

In high-temperature nematic phases, a conoscopic cross is observed which did not change upon rotation of the sample. The use of an additional circular polarizer revealed only one dark spot pointing to a uniaxial nematic phase (not shown). At approximately 50 °C, the uniaxial cross split into two separated isogyres (Figure 5C, D). With a circular polarizer, the two dark spots can be clearly seen (E, F) separately. Rotation of the sample by 45° in the orthoscopic mode causes strong change of the birefringence (A, B). These observations indicate a biaxial nature of the low-temperature monotropic nematic phase.

X-ray diffraction pattern of magnetic field aligned samples were recorded upon cooling the samples from the isotropic phase. Figure 6 shows the diffraction pattern of **1c** in the isotropic liquid, in the enantiotropic nematic at 139.0 °C and in the monotropic temperature range of the nematic phase at 75.0 and 45.6 °C. There are two halos in the isotropic phase; one corresponds to the typical mean separation of aliphatic chains of 4.5 Å and the other to a separation (17.5 Å) of shape-persistent molecules along the bisector. A reflection corresponding to the molecular long axis was not observed for this type of molecules. In the nematic phase, six diffuse reflections at (i) 15.1−14.3 Å, (ii) 4.5−4.2 Å, (iii) 10.3−9.9 Å, (iv) 5.2 Å, (v) 4.6−4.4 Å, and (vi) 3.1−3.0 Å are apparent at 139.0 and 45.6 °C. The peak (i) at 15.1 Å is positioned at the meridian and corresponds to the average separation along the bisector (cp. Figure 7). The second diffuse peak (ii) on the meridian at 4.5 Å arises from the mean transverse distance between hydrocarbon molecules, i.e., the separation in the direction normal to the plane of the conjugated scaffold. Simultaneous observations of reflections (i) and (ii) can be understood assuming a distribution of different biaxial

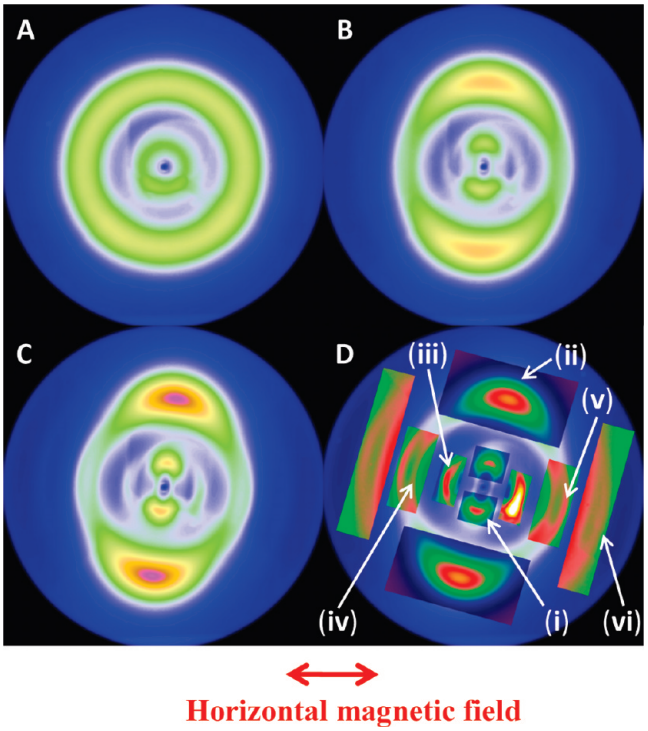

Figure 6. Temperature-dependent X-ray diffraction patterns of magnetic field aligned sample **1c** in (A) the isotropic phase, (B) the enantiotropic nematic phase at 139.0 °C and the monotropic nematic phase at (C) 75.0 and (D) 45.6 °C. The peaks in (D) are shown on different scales so that each of these are clearly visible.

domains (Figure 7) about the direction of the magnetic field. Within each domain, molecular long axes align along the magnetic field, whereas the director corresponding to the direction of the bisector has an orientation that varies randomly from domain to domain in a plane perpendicular to the magnetic field. Consequently, intensity of the peaks corresponding to the two length scales and originating from various domains probed by the X-ray beam lies along the meridian. All other peaks lie on the equator. The intensity of peak (iii) at ~10.3 Å corresponds to the

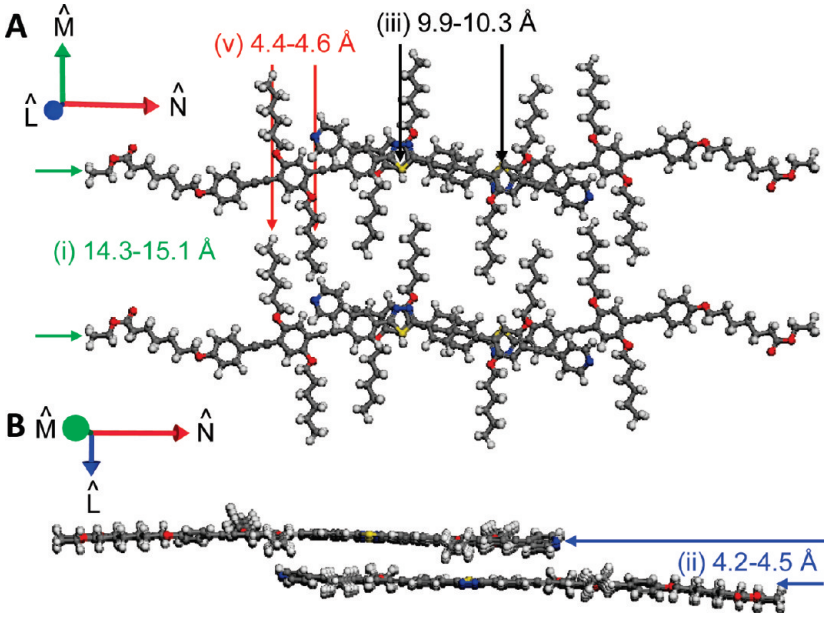

Figure 7. Model of a possible short-range order of **1c** in its nematic phase. The larger *d* spacings are values measured at 139 °C and the lower ones at 45.6 °C. The vectors **L**, **M**, **N** correspond to the molecular axes. (A) Orientation resulting in reflection (i) and all equatorial reflections. (B) Orientation leading to reflection (ii) and all equatorial reflections.

average separation of sulfur atoms along the long axis.[14] The diffuse reflection (v) at 4.6 Å along the equator may be attributed to the average distance between the lateral aliphatic chains oriented perpendicular to the magnetic field. Although the origin of the very diffuse and weak signals (iv) at 5.2 visible at all nematic temperatures is not known, it may belong to the average width of the six aromatic cores in the two arms of the molecule. The source of the weakest of the signals (vi) corresponding to ~3.1 Å is unclear. We will continue further investigations to better understand it and to rule out its being an experimental artifact.

The correlation lengths from the X-ray signals are estimated using $\xi = 2\pi/\mathrm{fwhm}$, (fwhm = full width at half-maximum), and are found to be 16.4, 8.3, 11.0, 9.5, 33.3, and 4.2 Å. Almost all of these liquidlike correlation lengths are in the range of one to three molecular units, which together with DSC and POM results point to the nematic nature of the phase. An exception is the signal (v) at 4.6 Å with a correlation length of seven to eight subunits. This might be explained by steric constrain and subsequently a relatively higher order of the lateral hexyl chains. Upon cooling to ambient temperature the correlation lengths increase but not significantly, the largest change being from 8 Å (<1 subunit) to 14 Å (1.8 subunits) for the reflection at 10 Å. This is consistent with the nematic nature of the phase over entire temperature range. However, the reflections become better defined along the meridian and at the equator, thus pointing to an increasing orientational order.

CONCLUSIONS

Shape-persistent thiadiazole mesogens **1** form nematic mesophases over a wide temperature range. They self-assemble homeotropically, presumably because the pyridyl units interact with the glass surface via hydrogen bonding. The nematic phase can be supercooled down to room temperature. At ~ 50 °C, conoscopy shows a splitting of the isogyres pointing to a possible biaxial nature of these nematic phases. Symmetrically substituted mesogens (e.g., **1f**) that were previously described did not reveal any sign of biaxiality. This can be rationalized by quantum-mechanical calculations showing a considerably larger dipole tilted with respect to the molecular long axis, which may help to stabilize the low temperature N_b phase. The nature of this phase is thus highly interesting. Work is in progress to study the precise nature of these nematic materials using dynamic light scattering, dielectric measurements, Raman, and ^{13}C solid-state NMR spectroscopy methods.

AUTHOR INFORMATION

Corresponding Author

*E-mail: Matthias.Lehmann@uni-wuerzburg.de. Fax: +49 (0)931 31−87350.

ACKNOWLEDGMENT

We thank the DFG for the financial support (LE 1571/2-1); H. Meier, A. Oehlhof and N. Hanold (University of Mainz) for FD MS and elemental analysis data; and J. Gutmann and M. Bach for the available X-ray equipment at the Max-Planck-Institute of Polymer Research, Mainz. This work was supported by the U.S. Department of Energy (USDOE) grant DE-SC0001412. The use of the Advanced Photon Source (APS) was supported by the U.S. Department of Energy, Basic Energy Sciences, Office of Science, under Contract W-31-109-Eng-38. The Midwest Universities Collaborative Access Team (MUCAT) sector at the APS is supported by the U.S. Department of Energy, Basic Energy Sciences, Office of Science, through the Ames Laboratory under Contract W-7405-Eng-82.

DEDICATION

§This paper is dedicated to the memory of our dear friend and colleague Alberto Marini, who passed away before the

submission of this manuscript. His scientific talents and enthusiasm will never be forgotten.

REFERENCES

(1) Vorländer, D. *Ber. Dtsch. Chem. Ges.* **1929**, *62*, 2831.
(2) Niori, T.; Sekine, T.; Watanabe, J.; Furukawa, T.; Takezoe, H. *J. Mater. Chem.* **1996**, *6*, 1231.
(3) Teixeira, P. I. C.; Masters, A. J.; Mulder, B. M. *Mol. Cryst. Liq. Cryst.* **1998**, *323*, 167.
(4) Luckhurst, G. R. *Thin solid Films* **2001**, *393*, 40.
(5) Freiser, M. J. *Phys. Rev. Lett.* **1970**, *24*, 1041.
(6) Yu, L. J.; Saupe, A. *Phys. Rev. Lett.* **1980**, *45*, 1000.
(7) (a) Hessel, F.; Finkelmann, H. *Polym. Bull.* **1986**, *15*, 349. (b) Severing, K.; Saalwächter, K. *Phys. Rev. Lett.* **2004**, *92*, 125501.
(8) (a) Fan, S. M.; Fletcher, I. D.; Gündogan, B.; Heaton, N. J.; Kothe, G.; Luckhurst, G. R.; Praefcke, K. *Chem. Phys. Lett.* **1993**, *204*, 517. (b) Hughes, J. R.; Kothe, G.; Luckhurst, G. R.; Malthete, J.; Neubert, M. E.; Shenouda, I.; Timini, B. A.; Tittelbach, M. *J. Chem. Phys.* **1997**, *107*, 9252. (c) Praefcke, K.; Brazillian, J. *Phys.* **2002**, *32*, 564.
(9) Madsen, L. A.; Dingemans, T. J.; Nakata, M.; Samulski, E. T. *Phys. Rev. Lett.* **2004**, *92*, 145505.
(10) Acharya, B. R.; Primak, A.; Kumar, S. *Phys. Rev. Lett.* **2004**, *92*, 145506.
(11) Tschierske, C.; Photinos, D. J. *J. Mater. Chem.* **2010**, *20*, 4263.
(12) Acharya, B. R.; Kang, S.-W.; Prasad, V.; Kumar, S. *J. Phys. Chem. B* **2009**, *113*, 3845.
(13) Francescangeli, O.; Samulski, E. T. *Soft Matter* **2010**, *6*, 2413.
(14) Yoon, H.-G.; Kang, S.-W.; Dong, R. Y.; Marini, A.; Suresh, K. A.; Srinivasarao, M.; Kumar, S. *Phys. Rev. E* **2010**, *81*, 051706.
(15) Lehmann, M.; Seltmann, J. *Beilstein J. Org. Chem.* **2009**, *5*, 73.
(16) Bates, M. A. *Chem. Phys. Lett.* **2007**, *437*, 189.
(17) Lehmann, M.; Seltmann, J.; Auer, A. A.; Prochnow, E.; Bendikt, U. *J. Mater. Chem.* **2009**, *19*, 1978.
(18) Frisch, M. J.; Frisch, M. J.; Trucks, G. W.; Schlegel, H. B.; Scuseria, G. E.; Robb, M. A.; Cheeseman, J. R.; Scalmani, G.; Barone, V.; Mennucci, B.; Petersson, G. A.; Nakatsuji, H.; Caricato, M.; Li, X.; Hratchian, H. P.; Izmaylov, A. F.; Bloino, J.; Zheng, G.; Sonnenberg, J. L.; Hada, M.; Ehara, M.; Toyota, K.; Fukuda, R.; Hasegawa, J.; Ishida, M.; Nakajima, T.; Honda, Y.; Kitao, O.; Nakai, H.; Vreven, T.; Montgomery, J. A., Jr.; Peralta, J. E.; Ogliaro, F.; Bearpark, M.; Heyd, J. J.; Brothers, E.; Kudin, K. N.; Staroverov, V. N.; Kobayashi, R.; Normand, J.; Raghavachari, K.; Rendell, A.; Burant, J. C.; Iyengar, S. S.; Tomasi, J.; Cossi, M.; Rega, N.; Millam, N. J.; Klene, M.; Knox, J. E.; Cross, J. B.; Bakken, V.; Adamo, C.; Jaramillo, J.; Gomperts, R.; Stratmann, R. E.; Yazyev, O.; Austin, A. J.; Cammi, R.; Pomelli, C.; Ochterski, J. W.; Martin, R. L.; Morokuma, K.; Zakrzewski, V. G.; Voth, G. A.; Salvador, P.; Dannenberg, J. J.; Dapprich, S.; Daniels, A. D.; Farkas, Ö.; Foresman, J. B.; Ortiz, J. V.; Cioslowski, J.; Fox, D. J. *GAUSSIAN 09 (Revision A.01)*; Gaussian, Inc.: Wallingford, CT, 2009.
(19) Hammersley, A. P.; Hanfland, M.; Fitch, A. N.; Häusermann, D. *High Pressure Res.* **1996**, *14*, 235.